Investigación *Revista Mexicana de Física* **39**, *No. 3 (1993) 409–427*

Analytical and numerical evaluation of the stress field during the neck formation in the cold drawing of thermoplastics

ALFREDO MÁRQUEZ LUCERO
Centro de Investigación Científica de Yucatán
Departamento de Polímeros, Km. 7 Ant. Carr. a Progreso
Ex-hacienda Xcumpich, Mérida, Yucatán, México

AND

CHRISTIAN G'SELL
Laboratoire de Métallurgie Physique & Science des Matériaux
(URA CNRS 155), Ecole des Mines
Parc de Saurupt, 54042 Nancy, France

Recibido el 9 de febrero de 1993; aceptado el 13 de abril de 1993

ABSTRACT. The effect of stress triaxiality on neck propagation during axisymmetric tension of thermoplastics was analyzed in terms of a modified "long wavelength" model of flow localization. The analysis involved a triaxiality factor $F_T(x_1)$ which expresses the radio of the mean effective stress to the mean axial stress in a given cross-section. Experimental values of $F_T(x_1)$ were determined in the case of high density polyethylene from (i) the influence of the initial shape of hour glass specimens on their apparent yield stress and (ii) from the analysis of the profile of a propagation neck. These results agree very well with the Bridgman factor which relates $F_T(x_1)$ solely to the relative curvature $N_c(x_1)$ of the profile. A finite element simulation of the necking process in polyethylene was also performed, which confirmed the qualitative aspects of the dependence of $F_T(x_1)$ on profile curvature. However, the computed factor was found to be systematically larger than the corresponding experimental value. This discrepancy could be attributed either to the limited number of finite elements in the mesh or, more fundamentally, to the neglect of the strain rate sensitivity, which was not taken into account in the constitutive relation chosen to model the material.

RESUMEN. El efecto del estado triaxial de esfuerzos durante la propagación del cuello en probetas axisimétricas de termoplástico es analizado en términos de una modificación al modelo "long wavelenght" comúnmente usado para estudiar la localización del flujo durante el régimen de inestabilidad plástica. Este análisis involucra la definición de un factor de triaxialidad $F_T(x_1)$, que relaciona el esfuerzo axial promedio con el esfuerzo efectivo promedio en una localidad dada. Los valores experimentales de $F_T(x_1)$ fueron determinados, para el caso del polietileno de alta densidad, usando dos técnicas, (i) a partir de la influencia de la geometría inicial sobre el esfuerzo de cedencia aparente, usando probetas en forma de reloj de arena; (ii) analizando el perfil del cuello durante su propagación. Estos resultados coincidieron muy bien con el factor de Bridgman, el cual relaciona $F_T(x_1)$ únicamente con la curvatura relativa $N_c(x_1)$ del perfil. Por otro lado, también se llevó a cabo una simulación, por elemento finito, del proceso de formación del cuello en polietileno. Simulación que confirmó los aspectos cualitativos de la dependencia del perfil sobre $F_T(x_1)$. Sin embargo, se encontró que el factor de triaxilidad obtenido por esta simulación es sistemáticamente superior al experimental. Esta discrepancia puede ser atribuida al limitado número de elementos en

la malla o, más fundamentalmente, al uso de un modelo cuya ecuación constitutiva es independiente de la velocidad de deformación.

PACS: 46.30.Jv; 46.30.Rc; 81.40.Ef

1. INTRODUCTION

The necking of ductile thermoplastics is a rather spectacular phenomenon usually present during the manufacture of polymeric fibers and films. This phenomenon can be easily observed when stress is gently applied to an unoriented ductile thermoplastic sample at a temperature inferior to their glass transition temperature (Tg). In this experiment a strain localization occurs very early producing the formation of a neck, such necking process, however, does not lead to rupture of the sample as in the case of metals. Instead the neck stops growing because in thermoplastics the rate of strain hardening compensate the cross-section decrease at this stage of the experiment. The neck propagates then over the length of the specimen. It has been shown that the neck propagation rate in several thermoplastics is nearly constant with time, and that the profile of the shoulder is merely translated along the sample axis [1, 2, 10, 30].

In order to control the neck growth during the industrial processes of thermoplastics it is important to understand the kinetics of the neck formation. This kinetics in thermoplastic samples is relatively complex and cannot be predicted only on the basis of a purely uniaxial analysis of plastic deformation [1-5], especially it is important to consider that the stress field during the necking of thermoplastics have an important triaxial nature due to the sharp profiles of the neck shoulders produced. Therefore, in the present work the "long wavelength" theory of necking (developed for metals) was modified by incorporating the effect of stress triaxility on the strain localization along the sample in a relatively simple way. This was achieved, for an axisymmetric sample of high density polyethylene, by evaluating a triaxiality factor that reflects the development of stresses in the radial and circumferential directions. The objective of this work is to determine the value of this triaxiality factor, $F_{\mathrm{T}}(x_1)$, employing an analytical and a numerical analysis. For such analysis were obtained the experimental data from two sets of tensile experiments (one composed of constant strain-rate tests, and other of constant streching-rate tests). Finally, the observed dependence of the triaxiality factor on the geometry of the neck profile was examined and discussed.

2. EXPERIMENTAL PROCEDURE

2.1. Material

Extruded rods 20 mm in diameter of a high density polyethylene (DFDY 6130 natural 77) manufactured by Union Carbide Limited, Canada, and extruded by Plastifab Inc. of Montreal, were chosen as the raw material for the present study. This material have a

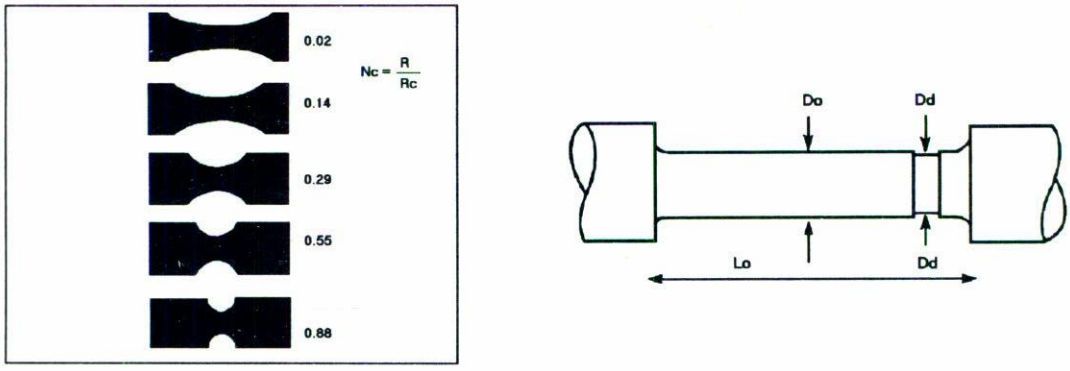

FIGURE 1. Polyethylene tensile specimens: a) Hourglass shaped specimens with decreasing relative curvature N_c (Type I), b) Axisymmetric specimens with a geometrical defect (Type II).

weight average molecular mass of 192,200 and a density of 0.956 ± 0.002 g/mc^{-3}. The following two types of specimens were machined from the previous rods:

Type I) The first type were hourglass shaped tensile specimens, with maximum and minimum radii of 3.5 and 1.5 mm, and longitudinal curvature radii from 1.70 mm to 35 mm (Fig. 1.a).

Type II) The second type were axisymmetrical tensile specimens with 8.0 mm in diameter (D_0), 40 mm length (L_0), with a geometrical defect at one extremity introduced in order to trigger a controlled neck initiation ($D_d = 7.89$ mm) (Fig. 1.b).

2.2. Tensile tests

All the tests were performed in an environmental chamber at a temperature of 25 ± 1°C. Principally two types of tests were performed: constant true strain-rate tensile tests and constant stretch-rate tests. The constant true strain-rate tensile tests were carried out according to a special method proposed by G'sell and Jonas [8]. These tests were performed employing the hourglass shaped specimens (Type I) tested in an Instron machine especially equipped with a diametral transducer and an exponential function generator. The true strain rate was fixed at 10^{-3} s^{-1}. The constant stretch-rate tensile tests were performed using the axisymmetrical specimens (Type II). These specimens were stretched at a rate of 4×10^{-4} mm/s in the previous Instron machine.

3. DEFINITION AND ANALYTICAL DETERMINATION OF THE TRIAXIALITY FACTOR IN POLYMERS

During the necking of an axisymmetric sample, the initially uniaxial stress field becomes triaxial because radial and circumferential stresses develop in the neck area to maintain the forces equilibrium. So as to obtain an unique normal stress-strain relationship it is necessarily to link the former uniaxial stress-strain data with the final triaxial ones. In order to perform this we need to evaluate the normal stresses on the stretch perpendicular directions. However, direct measure of such stresses is a very difficult task because the sample geometry becomes no homogeneous. Therefore, usually alternative methods of evaluation are preferred. An interesting method is to calculate a mean effective stress which have the same value in both stress fields (uniaxial and triaxial). This effective stress can be estimated multiplying the normal stress in the stretch direction $\bar{\sigma}_{11}$, by a "triaxiality factor" that takes into account the influence of the coexistent stresses in the other two directions. G'sell *et al.* [1, 2] was tentatively proposed that the triaxiality factor $F_T(x_1)$ can be evaluated as a first approximation from the expression

$$F_T(x_1) = \left[\left(1 + \frac{2}{N_c}\right) \ln\left(1 + \frac{N_c}{2}\right)\right]^{-1}, \qquad N_c = \frac{R}{R_c}, \tag{1}$$

derived previously by Bridgman [6], which relates the triaxiality effect solely to the local relative curvature (defined as $N_c(x_1) \equiv R/R_c$, where $R(x_1)$ are the local radius and $R_c(x_1)$ the local radius of curvature of the specimen profile, and x_1 is the axial position). Although it was shown that this approximation is capable to predict qualitatively all the stages of the neck formation and propagation [7], the derivation of the Bridgman factor suppose that the material is rigid-perfectly plastic and is rigorously valid only at the center of a diffuse symmetric neck. It is therefore of interest to consider the extent to which the formula for $F_T(x_1)$ would have to be modified for: i) thermoplastics which exhibit an elasto-plastic flow behavior with considerable strain hardening, and ii) asymmetric specimen profiles.

4. EXPERIMENTAL DETERMINATION OF THE TRIAXIALITY FACTOR IN POLYETHYLENE

4.1. Effect of stress triaxiality on the yield stress in hourglass shaped tensile specimen

From the constant true strain-rate tension tests, stress-strain curves $\bar{\sigma}_{11}(\bar{\epsilon}_{11})$ can be obtained using the hypothesis of constant volume. Here $\bar{\sigma}_{11} = P_1/\pi R^2$ is the cross section mean stress and $\bar{\epsilon}_{11} = 2\ln(R_0/R)$ is the local logarithmic axial strain. The curves $\bar{\sigma}_{11}(\bar{\epsilon}_{11})$ displayed in Fig. 2 show the influence of the initial curvature of the sample profile on the apparent stress-strain behavior of the specimens. It should be noted that the flow stress decreases gradually when the radius of curvature increases. Furthermore, the rupture of the specimen, which is dominated in polyethylene by cavitation mechanisms, occurs progressively earlier in specimens as the radius of curvature is reduced. These observations have been interpreted numerous times in terms of stress triaxiality [9, 10]. The stress field in specimens with a concave profile is not uniaxial since positive radial and circumferential

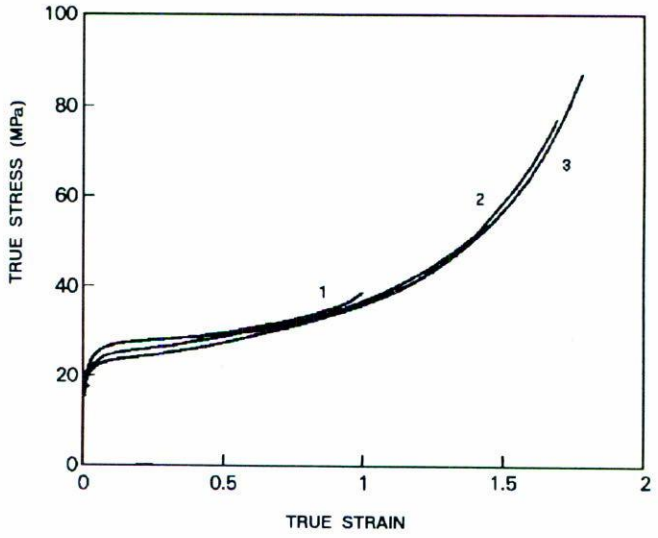

FIGURE 2. Influence of profile curvature on apparent flow behavior of polyethylene. 1: $N_c = 0.9$, 2: $N_c = 0.3$, 3: $N_c = 0.02$.

stress develop ab initio in the central cross section of the specimen. With reference to an uniaxial sample subjected to a given load, a triaxially stressed specimen experiences a smaller von Mises effective stress:

$$\sigma_{\text{eff}} = \frac{1}{\sqrt{2}}\left[(\sigma_{11} - \sigma_{22})^2 + (\sigma_{11} - \sigma_{33})^2 + (\sigma_{22} - \sigma_{33})^2\right]^{1/2}. \tag{2}$$

Also, the development of non axial stresses increases the hydrostatic stress, which favors the cavitation processes. In the present investigation, the profiles of a series of samples were photographed under load at the moment the true strain passed through $\bar{\epsilon}_{11} = 0.1$, that is just before the necking set in and the initial load drop. By means of this procedure, it was possible to correlate the true strain and the current radius of curvature in the course of a tensile test; in this way, the differences in flow stress could be ascribed solely to the differences in the stress triaxiality. In what follows, each specimen is referenced in terms of its "relative curvature" $N_c(x_1)$ which is defined as R/R_c, where $R_c(x_1)$ is the profile radius of curvature under load at the minimum cross section, of radius $R(x_1)$. An important case is that of the specimens with little initial curvature, which their flow stress closely corresponds to uniaxial state of stress, so that the true stress to which they are subjected at $\bar{\epsilon}_{11} = 0.1$ can be taken as the reference effective stress $\sigma_{\text{eff}}(\epsilon = 0.1)$. All the flow stress recorded with the hourglass samples were then compared with the above value, leading to the evaluation of the triaxiality factor $F_T = \bar{\sigma}_{\text{eff}}/\bar{\sigma}_{11}$. In Fig. 3, the dependence of $F_T(x_1)$ on the relative curvature of the samples is displayed. The experimental points show, with little scatter, a gradual decrease from 1 for $N_c \approx 0$ to about 0.8 at $N_c \approx 1.2$.

Since the above data concern the triaxiality effect in the plane of symmetry of the sample and were obtained just before of the load drop, they correspond closely to the

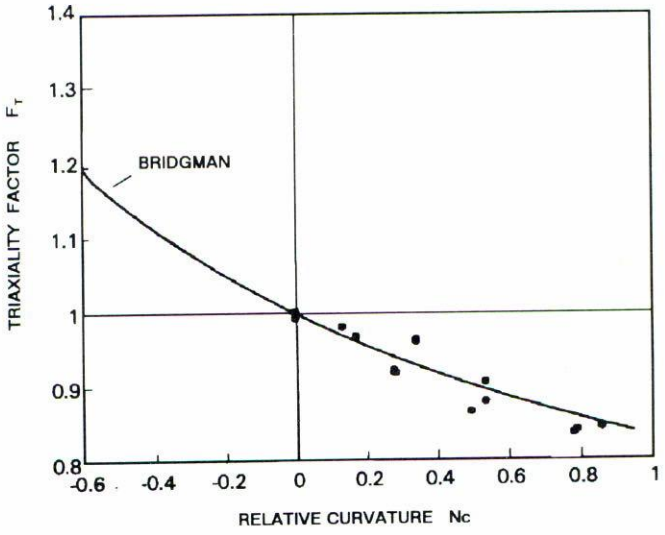

FIGURE 3. Influence of relative profile curvatue N_c on the experimental triaxiality factor F_T (points). The Bridgman factor is displayed for comparison.

conditions assumed by Bridgman [6] in the analytical derivation of this triaxiality factor. We have thus plotted the Bridgman factor $F_T(x_1) = [(1 + 2/N_c)\ln(1 + N_c/2)]^{-1}$ (solid curve) for comparison with the experimental points in Fig. 3. It is evident that the argument is very good over the whole range of curvatures, and that these curvatures extend over a greater range than the maximum curvatures measured in naturally necked specimens of polyethylene.

4.2. Determination of the effective stress-strain behavior of polyethylene at constant true strain rate

On the basis of the above results, the effective stress-strain curve for polyethylene was deduced as follows. Although in the present work the experimental validity of the Bridgman expression for the triaxiality factor was established at $\bar{\epsilon}_{11} = 0.1$ only, it was assumed that the relation continues to be valid at larger strains in the plane of minimum cross section. This assumption is presumably reasonable as long as the curvature remains moderate and as long as the strain hardening due to molecular orientation does not lead to drastic changes in the triaxial stress distribution in the center of the neck.

The evolution of the local profile at the neck was recorded with a TV camera during the stretching at 25°C of a cylindrical polyethylene sample at a constant true strain rate $\dot{\bar{\epsilon}}_{11} = 10^{-3}\ s^{-1}$. From this record, is was found that the relative curvature $N_c(x_1)$ remained small, attaining a maximum value of 0.38. The evolution of the triaxiality factor was then computed from the Bridgman formula. It is 1.0 at yielding, decreases to a minimum value of 0.92 at $\bar{\epsilon}_{11} = 0.95$ and then returns to 1.0 as the neck becomes stabilized at larger

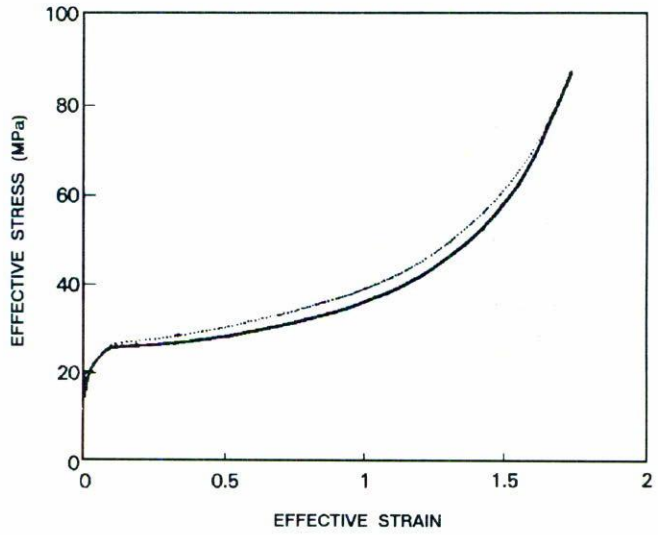

FIGURE 4. Effective stress-strain behavior of high density polyethylene (solid curve) deduced by applying the triaxiality correction to the experimental curve (dotted line).

strains. The effective stress-strain curve was computed in this way and an example is displayed in Fig. 4 (solid line) together with the uncorrected flow curve (dotted line).

The effective stress-strain curve derived using the above procedure can be considered to represent the intrinsic plastic behavior of the material under conditions of: i) constant temperature, ii) constant effective strain rate, and iii) uniaxial deformation.

Similar experiments using a photographic camera were performed at a variety of strain rates; the results obtained were published elsewhere [8]. The strain rate sensitivity $m = (\partial \ln \sigma_{\text{eff}} / \partial \ln \dot{\epsilon})\epsilon$, T was evaluated from these data and found to equal about 0.075.

4.3. Effect of stress triaxiality on neck propagation

As mentioned above, it has been demonstrated in the literature [1, 2, 11, 12] that necking occurs very early when ductile thermoplastic specimens containing a geometrical defect are stretched. However, unlike the behavior in metals, such necking does not lead to localized rupture if the stretching is performed under isothermal conditions. Instead the neck stops growing because, in thermoplastics, the rate of strain hardening exceeds the rate of decrease in area of cross-section at this stage of the experiment. The neck is then propagated over the length of the specimen, through regions which were initially free of any cross-section defect. It was shown that the propagation rate is nearly constant with time, and that the profile of the shoulder (Fig. 5) is merely translated along the sample axis.

The propagation of a neck along stretched polymer is thus an interesting problem in plastic instability and flow localization. It demonstrates unambiguously that the presence of a geometric or mechanical defects is not necessary for the flow to localize at a given

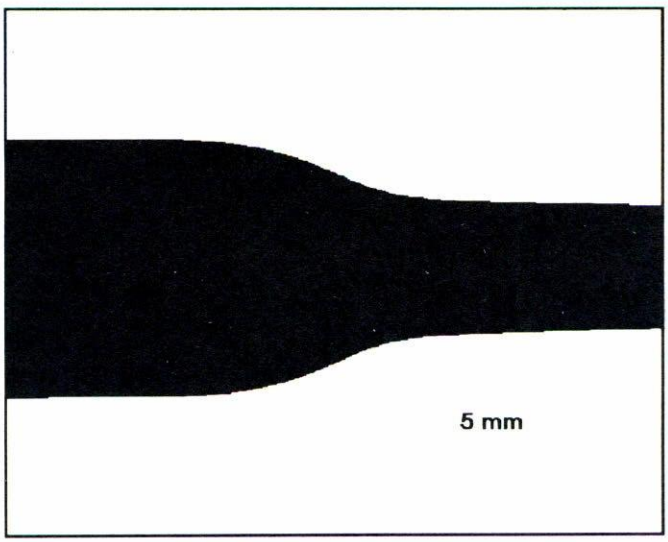

FIGURE 5. External profile of a propagating neck shoulder during the stretching of a polyethylene specimen.

cross section. It shows instead that stress triaxiality is the factor controlling isothermal neck propagation in thermoplastics. We will demonstrate below that the analysis of the profile of a propagating neck can provide an estimate of the triaxiality factor, not only in regions with concave curvature, but also in those regions of the shoulder with a convex profile.

In two previous papers [1, 2], we revised the classical long wavelength treatment of flow localization [5] by incorporating the effect of stress triaxiality. This "modified long wavelength" analysis resulted in the following equation for the case of a uniformly propagating neck:

$$\bar{m}\lambda' = (1 - \gamma - \bar{m}) + \frac{\partial \ln F_T(x_1, t)}{\partial x_1}. \tag{3}$$

Here x_1 is the axial location of the cross section in eulerian coordinates, $\lambda = \partial\epsilon(x_1, t)/\partial x_1$ is the strain gradient, and $\lambda' = \partial\lambda(x_1, \epsilon)/\partial\epsilon$ express the rate of flown localization. The strain hardening coefficient $\gamma = (\partial \ln \sigma_{\text{eff}}/\partial\epsilon)\dot{\epsilon}, T$ and the mean strain-rate sensitivity $m = (\partial \ln \sigma_{\text{eff}}/\partial \ln \dot{\epsilon})\epsilon, T$ characterize the plastic flow behavior of the polymer. The second term on the RHS corresponds to the triaxiality correction.

In the case of the propagating neck displayed in Fig. 5, the profile, $R(x_1)$, of the specimen was analyzed by means of a digital image system interfaced with a microcomputer. The strain distribution $\bar{\epsilon}_{11}(x_1)$ was then computed with reference to the uniform initial radius R_0. The two terms $\lambda(x_1)$ and $\lambda'(x_1)$ were evaluated in this way all along the profile; the values of $\gamma(\epsilon)$ and $\bar{m}$ were determined from separate experiments. The triaxiality term $\partial \ln F_T/\partial x_1$ was then calculated. Integration over x_1 led to the axial dependence of the triaxiality factor $F_T(x_1)$ and finally to the variation of $F_T(N_c)$ with the local relative curvature of the profile $N_c = R(d^2R/dx_1{}^2)^2(1 + (dR/dx_1)^2)^{-3/2}$, which is illustrated in

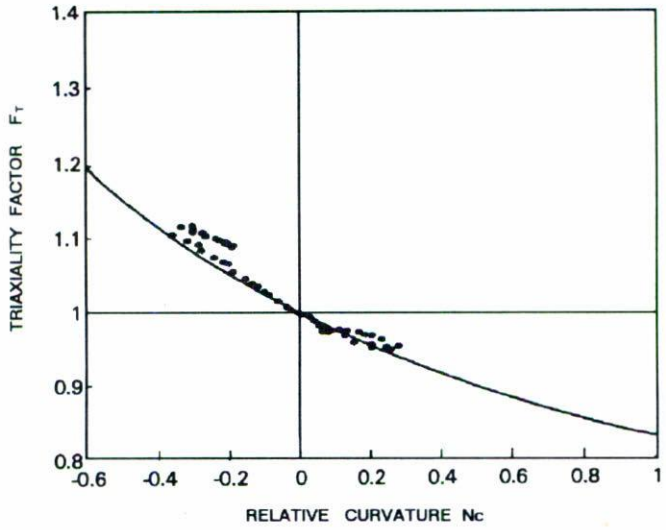

FIGURE 6. Influence of relative curvature N_c on the triaxiality factor F_T determined from the analysis of the neck profile in Fig. 5. The solid curve represents the Bridgman factor.

Fig. 6. This plot covers a range of curvatures from +0.3 to −0.4 and therefore represents the effect of stress triaxiality in both the concave as well as convex regions of the profile. The range of negative $N_c(x_1)$ values corresponds to strains up to about 1.0 (which occur at the inflection point of the profile) while the positive curvatures are found in the regions with $1.0 < \bar{\epsilon}_{11}(x_1) < 1.8$. We have also plotted in Fig. 6 the classical Bridgman factor versus $N_c(x_1)$. Although this factor was originally derived for a symmetrically concave neck, it has been shown [7] that the expression also remains valid for symmetrically convex bulges. In the present case, the convex shoulder profile exhibits a non-zero slope but we retained the Bridgman formula as a tentative approximation.

It should be noted that there is a good agreement between the experimental triaxiality factor and the Bridgman formula. It is also evident that the Bridgman formula underestimates slightly the experimental values.

5. FINITE ELEMENT COMPUTATION OF STRESS TRIAXIALITY DURING THE NECKING OF AN AXISYMMETRIC TENSILE SPECIMEN

5.1. Computing method

A finite element program was developed in order to determine the distribution of strains and stresses in a polymer rod subjected to axial stretching. This program employs a technique, applicable to materials obeying an elastoplastic constitutive relation, that has been capable of simulating large deformations of metal structures [13-16]. In this technique the equilibrium rate at arbitrary amounts of deformation is given by the virtual work

equation and the equilibrium equation is then written in the following form [17]:

$$\int \left[\sigma_{ij}{}^{\mathrm{J}}\,\delta\dot{\epsilon}_{ij} - \tfrac{1}{2}\sigma_{ij}\delta(2\dot{\epsilon}_{ik}\dot{\epsilon}_{kj} - \partial_i v_k \cdot \partial_j v_k)\right] dv = \int \dot{F}_i\,\delta v_i\,dv + \int \dot{P}_i\,\delta v_i\,ds, \tag{4}$$

where $\sigma_{ij}{}^{\mathrm{J}}$ is the Jaumann derivative of the stress tensor, and $\dot{F}_i$ and $\dot{P}_i$ are the time derivatives of the body and surface forces. The constitutive law for elastic loading is

$$\dot{\epsilon}_{ij} = \frac{1+\nu}{E}\sigma_{ij}{}^{\mathrm{J}} - \frac{\nu}{E}\delta_{ij}\sigma_{kk}{}^{\mathrm{J}}, \tag{5}$$

where ($E = 87$ MPa) and ν ($= 0.35$) are the Young's and Poisson's module and δ_{ij} is the Kronecker delta. For loading at yield, the constitutive law changes to

$$\dot{\epsilon}_{ij} = \frac{1+\nu}{E}\sigma_{ij}{}^{\mathrm{J}} - \frac{\nu}{E}\delta_{ij}\sigma_{kk}{}^{\mathrm{J}} + \frac{9}{4}\frac{\sigma'_{ij}\sigma'_{k\ell}\sigma_{k\ell}{}^{\mathrm{J}}}{h\sigma_{\mathrm{eff}}^2}, \tag{6}$$

here σ'_{ij} is the deviatoric stress and $h(\epsilon)$ is the tangent modulus of the effective stress-strain curve whose shape was modeled from the experimental curve of Fig. 4 by fifteen successive segments. Moreover, the following simplification were introduced in the model: i) the rounded transition from the elastic to plastic flow of the stress-strain curve was modeled by a sharp elastic limit, ii) even though the strain rate sensitivity of the polyethylene is important $m = 0.075$ it was not introduced into the computation due to the limitations of time and cost. Nevertheless, the expected effect of rate sensitivity will be discussed qualitatively in the section that follows.

For the present work, a specimen of cylindrical symmetry was modeled employing a mesh with 24 quad elements, as illustrated in Fig. 7. Because of the symmetry, only one quadrant of the specimen had to be modeled. The initial specimen length was 20 mm and the nominal radius 3 mm. At the central cross-section of the specimen, a V–shaped geometric defect was introduced with a minimum radius of 2.95 mm and a width of 2 mm.

Eight peripheral nodes were associated with each element and the stresses and strains were computed at the four Gauss points. The boundary conditions were the usual ones for axisymmetric solids and the ends were considered as being shear-free. An Eulerian finite element equation was writte as

$$\big([K_c] + [K_s]\big)\{\varphi\} = \{\dot{P}\}, \tag{7}$$

where $\{\varphi\}$ is a stream function and $[K_c]$ and $[K_s]$ represent the usual small displacement stiffness matrix and the initial strain matrix. The solution was achieved by the Cholesky decomposition method in 501 successive steps, for a total specimen elongation of 4.8 mm, (24%). The first step, which is larger than the following ones, corresponds to the elastic loading of the sample; at each step, the complete strain and stress tensors were determined at each Gauss point, together with the effective strain and stress.

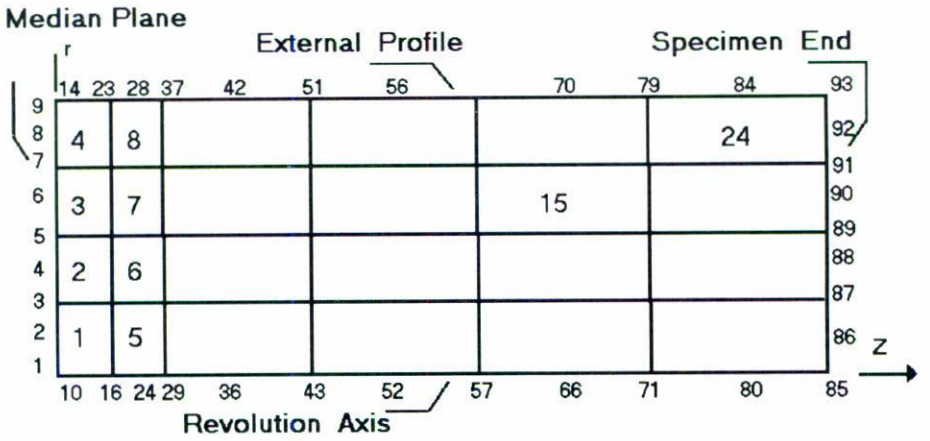

FIGURE 7. Finite element mesh employed to model the present axisymmetric tensile specimen (only one quadrant is represented). The geometric defect is visible at element number 4 between nodes 9 and 14.

5.2. Computation results

The load-elongation curve obtained by integrating the axial stress $\bar{\sigma}_{11}$ over the end cross-section is displayed in Fig. 9. It shows an early maximum followed by the gradual decrease of the load. This behavior is associated with the development of a symmetrical diffuse neck which is displayed in terms of the evolution of the finite element mesh (Fig. 8). When the elongation is about 4 mm (10%), the load-elongation curve reaches a plateau, while the mean strain in the central cross-section of the sample tends to stabilize, as observed experimentally. It should be noted that the finite element mesh in Fig. 9e (501 steps) is highly distorted, due to the limited number of elements near the central cross-section, so that the computation was not continued beyond this elongation (24%). Nevertheless, some quantitative information was extracted from the results of this computation, concerning mainly: (i) The external profile of the simulated specimen during the stretching process, and (ii) the distribution of strains and stresses in the volume of the material.

The evolution of the computed radius *vs.* axial coordinate $R(x_1)$ was analyzed quantitatively after interpolation by the cubic spline method. It is evident from Fig. 9 that stretching the specimen provokes the development of a marked diffuse neck centered on the original geometric defect. However it can be seen that the width of the neck is much greater than the actual width of the initial defect. The shape of the stretched rod can be decomposed into three parts: (i) in the heavity strained portion of the neck, that is near the original defect, the profile exhibits a concave curvature; ii) conversely, at the two shoulders of the neck the curvature of the profile changes its sign gradually and becomes convex; iii) finally near the ends of the rod, the overall strain tends to zero and the curvature of the profile gradually disappears. The shape of the sample was analyzed in terms of the local slope $dR(x_1)/dx_1$ and the relative curvature $N_c(x_1)$. It is clear that the relative curvature is equal to zero in two locations: i) near the specimen ends where the slope is also zero; and ii) at the point of inflection of the neck shoulder. The looped

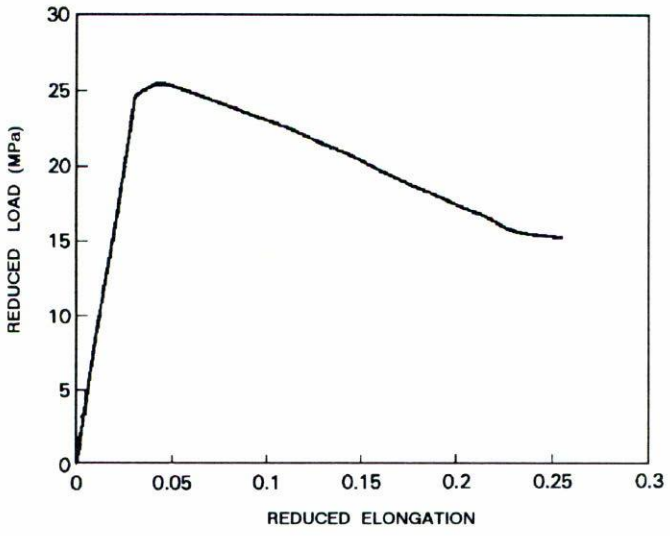

FIGURE 8. Load (per unit cross section) *vs.* reduced elongation, resulted from the numerical simulation.

curves in Fig. 10 show, at four steps of the computation, that the negative curvature at the shoulders becomes more and more marked (with values reaching $N_c(x_1) = 0.4$ at step 501) while the curvature near the defect decreases gradually.

The distribution of strains within the simulated specimen was determined by interpolating the computed data between the Gauss points by means of a two dimensional cubic spline. We were interested particularly in comparing, in plane cross sections normal to the axis, the difference between the local effective strain $\epsilon_{\text{eff}}(R)$ and the apparent "true" strain $\epsilon_{11} = 2\ln(R_0/R)$. It was found that $\epsilon_{\text{eff}}(R)$ decreases with increasing $R(x_1)$ near the center of the neck, while it increases slightly at the shoulders. In contrast, the effective strain is fairly constant over sections which correspond to zones where the external profile is not curved (*i.e.* at the inflection point of the $R(x_1)$ curve and near the ends of the specimen). This discrepancy between the apparent uniaxial strain and the effective strain has been discussed previously in the literature for the case of metals [18]. It is associated with the different strain paths followed by material elements located at different initial radii and axial coordinates.

The distribution of stresses was analyzed by a similar interpolation method. The evolution of σ_{11}, σ_{22}, σ_{33} and σ_{12} were considered, together with those of the effective stress σ_{eff}. We focussed our attention again on the distribution of stresses in plane cross sections normal to the specimen axis. From this analysis it appears that non axial stresses ($\sigma_{22} = \sigma_{33}$, σ_{12}) develop in the specimen as soon as the neck appears. The systematic presentation of the distribution and evolution of these components would be rather cumbersome. More relevant to the objectives of this work is a comparison of the axial and effective stresses in various cross sections. Since σ_{11} and σ_{eff} are strictly in the uniaxial case, the difference between these two quantities is a measure of the degree of triaxiality. The curves in Fig. 11

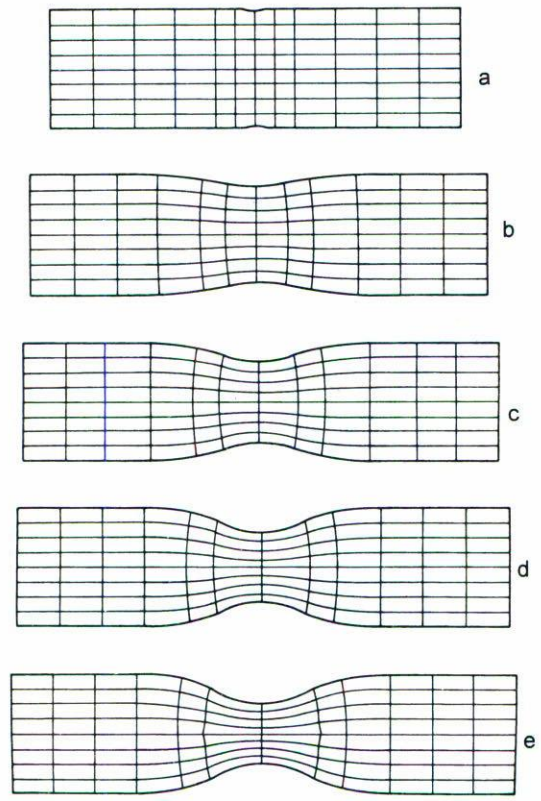

FIGURE 9. Finite element simulation of the extension of an axisymmetrical tensile specimen of polyethylene. a: Step 0; $\Delta L = 0$. b: Step 201; $\Delta L = 0.113$. c: Step 301; $\Delta L = 0.155$. d: Step 401; $\Delta L = 0.198$. e: Step 501; $\Delta L = 0.240$.

illustrate this analysis for eight cross-sections at step 301. It is evident that in the central plane of the neck where the axial and tangential stresses are both positive, the axial stress σ_{11}, is significantly larger than effective stress, except at the surface where the normal (radial) stress disappears. Conversely, at the shoulder of the neck $x_1 = 3$ to 5 mm, the non-axial stresses become negative and σ_{11} is smaller than σ_{eff}, again except in a very narrow zone near the surface. It is of particular importance that at the inflection point of the external profile $x_1 = 2$ mm, the σ_{11} and σ_{eff} curves are nearly superimposed and horizontal, which shows that the local state of stress is close to uniaxial, as it is at the end of the specimen (see curves for $x_1 = 9$ mm).

A general estimate of the effect of stress triaxiality can be obtained from the mean value of the ratio $\bar{\sigma}_{\text{eff}}/\bar{\sigma}_{11}$ calculated by the integration of $\sigma_{\text{eff}}(R)$ and $\sigma_{11}(R)$ in each cross section. This definition is fully consistent with the "triaxiality factor" $F_{\text{T}}(x_1)$ defined in the previous section. The $F_{\text{T}}(x_1)$ *vs.* x_1 curve displayed in Fig. 12 shows unambiguously, for step 301, that $F_{\text{T}} < 1$ in the center of the neck, $F_{\text{T}} > 1$ at the neck shoulders

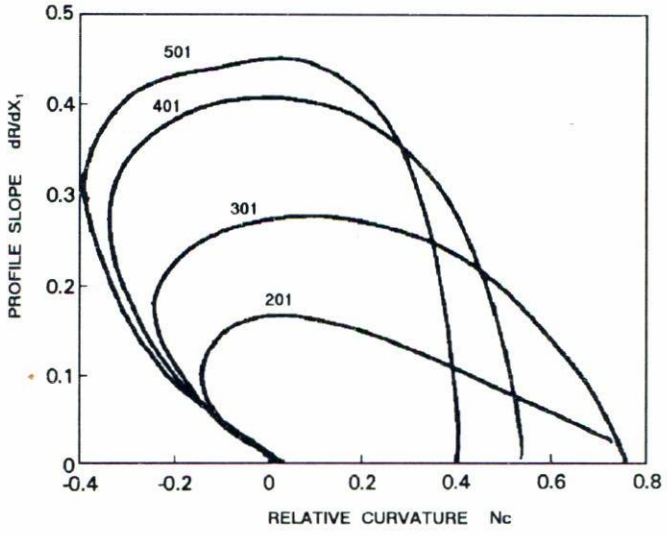

FIGURE 10. Correlation between external slope and relative curvature along the simulated profile at different stages (steps 201, 301, 401 and 501). Note the gradual increase in profile slope at the point of inflection ($N_c = 0$) as the simulation proceeds.

and $F_T \approx 1$ in the regions where the curvature cancels. Finally, the correlation between $F_T(x_1)$ and the relative curvature $N_c(x_1)$ is illustrated in Fig. 13 in which all the present results are displayed together. It is evident that the computed values of $F_T(x_1)$ generally decrease with increasing relative curvature $N_c(x_1)$ at all stages of the simulation. (The considerable scatter can be attributed to the limited number of finite elements and to the imperfection of the interpolation procedures). It is worthy of note that the triaxiality factor is essentially dependent on the relative curvature $N_c(x_1)$ and is influenced to only a minor extent by the local slope dR/dx_1; this can be deduced from the observation that all the points corresponding to $N_c = 0$ display the same triaxiality factor $F_T \approx 1$, even though the associated slopes vary from 0 to 0.45 (at the point of inflection). Comparison can be made again with the Bridgman factor (solid curve). It is of interest that both the computed and Bridgman factors show the same general evolution. In the range of positive curvatures, the computed values of $F_T(x_1)$ are in good agreement with the Bridgman approximation. However, in the range of negative (convex) curvatures, the finite element results predict a level of stress triaxiality which is much larger than the values calculated from the Bridgman formula.

6. DISCUSSION

In the first attempts several authors based their models of flow localization in tension [3, 4], on very simple assumptions: i) static equilibrum, ii) isothermal deformation, and iii) a uniaxial state of stress. Although this rough level of approximation was enough to predict

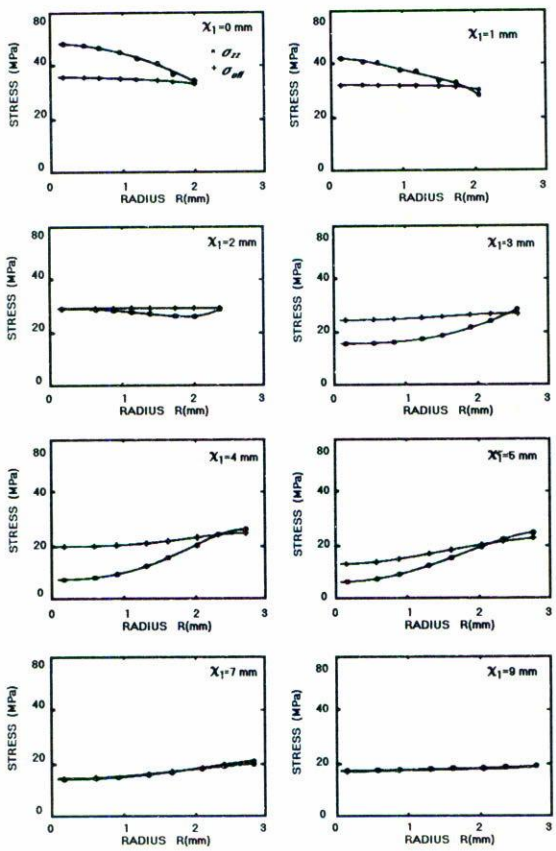

FIGURE 11. Dependence on $x_2(r)$ of the local axial ($\bar{\sigma}_{22}$) and effective ($\bar{\sigma}_{\text{eff}}$) stress at 8 different cross-section at step 301.

most of the qualitative aspects of neck formation and development starting from an initial defect, it has been demonstrated [19, 20] that it fails to model the kinetics of necking in cases such as fast tensile testing or the deformation of low thermal conduction materials, examples which exhibit inertia and self-heating effects, respectively. However, even if these artifacts are avoided by pulling the sample very slowly, it has been shown [21] that the strain gradients which are observed in practice are generally smaller than those expected from the uniaxial theories. The natural evolution of a growing inhomogeneity is to spread itself over the neighboring zones of the specimens. In terms of the present treatment, this phenomenon is associated with a stress triaxiality effect, which is responsible for the transmission of non axial constraints between neighboring cross sections. Experimental evidence of this effect is widespread in the literature but it is remarkable that neck propagation as such has not often been clearly interpreted in terms of stress triaxiality in the neck of polymers, a phenomenon which has been invariably attributed to adiabatic heating as recently as the 1960's when it was shown unambiguously [11] that it could be observed at infinitesimal pulling rates as well.

Several papers concerned with the analytical and numerical investigation of strains and

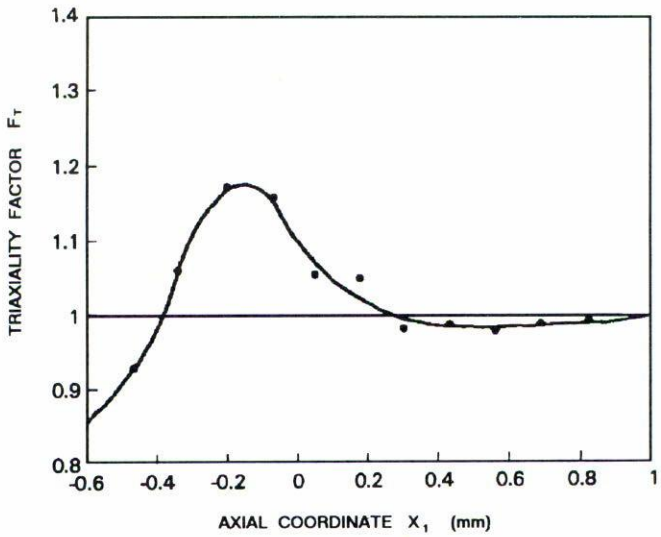

FIGURE 12. Dependence of computed triaxiality factor F_T on axial location in the simulated specimen at step 301.

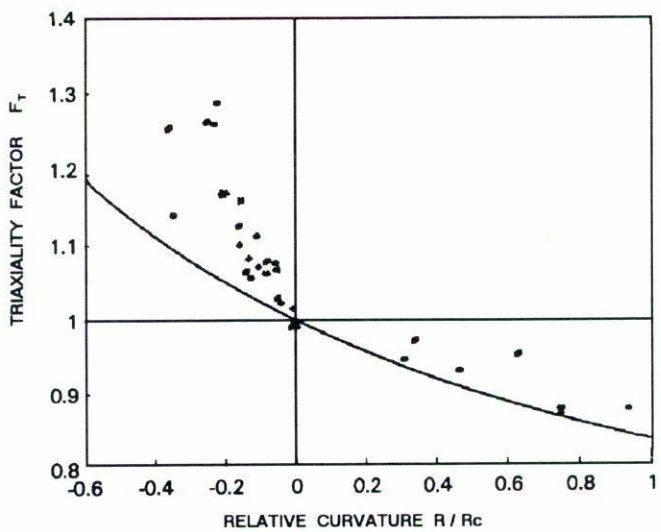

FIGURE 13. Influence of relative curvature N_c on the triaxiality factor F_T determined from the stress distribution at four stages of the computation.

stress in necked bars [10, 22, 23], attest to the complexity of the triaxiality problem. This is in part because material elements situated at the same initial x_1-coordinate in a cylindrical bar are brought to different positions while necking is proceeding. The occurrence of the

above phenomenon is revealed by the curvature of the originally plane cross section in the finite element diagrams. Neighboring material elements also experience different strain paths in the way to their current state of stress. Furthermore, the strain rates evolve in a different manner in the various regions of a given cross-section. The triaxiality factor $F_T(x_1)$ may therefore depend, not only on the geometry of the sample, but also on the constitutive behavior of the material and even on the complete history of each specimen.

Although an accurate assessment of the effects of triaxiality must include all the aspects presented above, simple approximate solutions remain of considerable interest. The classical literature provides various triaxiality factors applicable either to axisymmetric rods or sheets deformed in plane strain [6, 24-27]. The Bridgman formula used above appears to be the most useful for round specimens. It is based on the following assumptions: i) that the neck is symmetrically concave with a small relative curvature ($N_c \ll 1$); ii) that the material is isotropic and rigid-plastic and does not display strain hardening; iii) that the flow stress is insensitive to strain rate. Under these conditions, it was shown that the triaxiality factor is a function of $N_c(x_1)$ only. Now, it can be readily shown that the profile need not be concave for the Bridgman relations can be set aside. However, the remaining assumptions suggest that the Bridgman formula may not apply to unsymmetric parts of the neck (*e.g.* the neck shoulders) in polyethylene which displays strain rate sensitivity and anisotropic strain hardening. Nevertheless, it is evident from Figs. 3 and 6 that in practice, the Bridgman factor takes very well into accunt the experimental triaxiality effects both at the shoulder of a neck. This unexpected agreement can be interpreted in two different ways. On the one hand, it may be conjectured that not all of Bridgman's assumptions are equally critical. For example, according to published calculations [27], the development of non axial stresses in sheets is only slightly affected by the non zero slope of the external profile and the curvature indeed appears to be the leading geometric parameter. According to a second line of argument, it is possible that the departures from the assumptions could counterbalance each other. For example, at very large specimen extensions, the neck has propagated far away from the central regions and the profile is again perfectly cylindrical. Under these conditions, it has been shown [22, 23] that the stress distribution does not return to perfect uniaxiality since material elements situated at different radii do not follow the same strain path. According to the theoretical analyses of these authors, a triaxiality factor greater than 1 (by about 5%) should be observed in this state, while the simple Bridgman formula gives a value of 1. However it is possible that the development of a fiber-like texture in highly drawn polyethylene [28], with the fiber axis parallel to the drawing direction, favors stress uniaxiality in the necked region and thus brings the experimental $F_T(x_1)$ closer to 1 as indicated by the prediction for ideally isotropic materials.

Of considerable importance is the large discrepancy observed between the experimental data (Figs. 3 and 6) and the results of the finite element simulation (Fig. 13). This discrepancy may have two causes. First, the results of the modeling may suffer from inaccuracies associated with the relatively large size of the finite elements which were used. This affects the intrinsic precision of the stress computed at each node from the displacements of its peripheral nodes. Furthermore, the accuracy of the interpolation procedure, which was used to compute the stresses in the specimen cross sections, is lower when there are fewer elements, especially at large strains. Thus the performance

of the computation could be improved at the price of a finer mesh and more times of iteration for correcting the unbalanced forces.

An alternative cause of the discrepancy may be that strain rate sensitivity was neglected in the finite element model, which used a simple elasto-plastic flow equation instead. It is evident that the computation predicts a kinetics of necking which are more abrupt that the experimental process for the same specimen geometry [29]. In the computation, the neck formation process and thus the decreasing portion of the load-extension curve (Fig. 8), extends over and elongation range of about 20%. By contrast, in the experiment, neck formation ends at an elongation of about 55%. The strain gradients also develop earlier and more abruptly in the finite element computation. the delaying and smoothing effect of strain rate sensitivity in flow localization is well know [1-5]. It is clear that neglecting it in the present modeling is likely to have a detectable influence on the stress triaxiality. Although the magnitude of this influence is not yet know, it is probable that the accuracy of finite element analyses will be improved when more realistic flow equations, in which allowance is made for rate sensitivity, are employed. For this reason, we are concurrently modifying our procedures so that visco-elasto-plastic constitutive equations can be used.

7. CONCLUSIONS

It can be concluded that: i) triaxial stresses play a significant role in the propagation of isothermal neck; ii) the triaxiality factor is primarily dependent on the relative curvature of the external profile, with other parameters such as the profile slope and the nature of the constitutive relation playing much smaller parts; iii) the Bridgman formula gives a good first approximation of the triaxiality factor in the region of both positive and negative curvatures, and is therefore of practical value for the description of the cold drawing of polymers; iv) rate insensitive finite element simulations are only capable of reproducing the qualitative aspects of neck propagation and the use of visco-elasto-plastic constitutive relations will probably be required before increased accuracy can be attained.

ACKNOWLEDGEMENTS

The authors wish to thank Professor J.J. Jonas (McGill University, Montreal, Canada) for useful suggestions, and to Mr. Pedro Fuentes and Mr. Juan Canul (CICY) for technical support.

REFERENCES

1. C. G'Sell, N.A. Aly-Helal, and J.J. Jonas, *J. Mater. Sci.* **18** (1983) 1731.
2. C. G'Sell, A. Márquez-Lucero, P. Gilormini, and J.J. Jonas, *Acta Metall.* **33** (1985) 759.
3. E.W. Hart, *Acta Metall.* **15** (1967) 351.
4. J.J. Jonas, R.A. Holt, and C.E. Coleman, *Acta Metall.* **24** (1976) 911.
5. U.F. Kocks, J.J. Jonas and H. Mecking, *Acta Metall.* **27** (1979) 419.
6. P.W. Bridgman, *Trens. Am. Soc. Metals.* **32** (1944) 553.

7. C. G'Sell and N.A. Aly-Helal, *Proc. Int. Conf. on Deformation, Yield and Fracture of Polymers*, Cambridge, 1-4 April, (1984).
8. C.G'Sell and J.J. Jonas, *J. Mater. Sci.* **14** (1979) 583.
9. E.R. Parker, H.E. Davis, and H.E. Flanigan, *Proc. Am. Soc. Test. Mat.* **49** (1946) 1159.
10. V. Tvergaard and A. Needleman, *Acta Metall.* **32** (1984) 157.
11. P.I. Vincent, *Polymer* **1** (1960) 7.
12. G. Meinel and A. Peterlin, *J. Polymer Sci.* **A29** (1971) 67.
13. Ji Xing and Ying Jiaju, *J. of Xi'an Jiaotong University* **3** (1979) 45.
14. L.B. Freund, *Int. J. Solid Structures* **6** (1970) 1193.
15. H.D. Hibbitt, P.V. Marcal, and J.R. Rice, *Int. J. Solid Structures* **6** (1970) 1069.
16. R.M. McMeeking and J.R. Rice, *Int. J. Solid Structures* **11** (1975) 601.
17. J.R. Osias and J.L. Swedlow, *Int. J. Solid Structures,* **10** (1974) 321.
18. A.S. Argon, J. Im, and A. Needleman, *Metall. Trans.* **A6** (1975) 815.
19. C. Fressengeas and C. Molinari (to be published).
20. G. Ferron, *Mater. Sci. Eng.* **49** (1981) 241.
21. S.L. Semiatin and J.J. Jonas, *Formability and workability of metals: plastic instability and flow localization*, A.S.M., Metals Park, Ohio (1984), 125.
22. J.W. Hutchinson and K.W. Neale, *J. Mech. Phys. Solids* **31** (1983) 405.
23. K.W. Neale and P. Tugcu (submitted to *J. Mech. Phys. Solids.*
24. E. Siebel, *Werkstoffaus* **71** (1925) 5.
25. N.N. Davidenkov and N.I. Spiridonova, *Proc. Amer. Soc. Test. Mater.* **46** (1946) 1147.
26. P.W. Bridgman, *Studies in large plastic flow and fracture*, Harvard Univ. Press, Cambridge (1964) 36.
27. A.K. Ghosh, *Acta Metall.* **25** (1977) 1413.
28. A. Peterlin, *J. Polymer Sci.* **C15** (1966) 427.
29. A. Souahi (unpublished work).
30. A. Márquez, Doctoral thesis, Nancy, France.